Asian Journal of Chemistry; Vol. 38, No. 3 (2026), 629-635
ASIAN JOURNAL OF CHEMISTRY
https://doi.org/10.14233/ajchem.2026.33141

Tuning of TiO_2 Photocatalytic Efficiency: Insights into Hydrothermal and Sol-Gel Synthesised Undoped and Rare Earth-Doped Nanoparticles

SUNANDA[1], POOJA NARWAL[2], PAMELA SINGH[3] and BRIJNANDAN S. DEHIYA[1,2,*]

[1]Department of Chemical Engineering, Deenbandhu Chhotu Ram University of Science and Technology, Murthal-131039, India
[2]Department of Materials Science & Nanotechnology, Deenbandhu Chhotu Ram University of Science and Technology, Murthal-131039, India
[3]Department of Biotechnology, Deenbandhu Chhotu Ram University of Science and Technology, Murthal-131039, India

*Corresponding author: E-mail: brijnandan.che@dcrustm.org

Received: 5 December 2024 *Accepted*: 24 December 2025 *Published online*: 6 March 2026 AJC-22281

This study investigates the synthesis, characterisation and photocatalytic performance of TiO_2 nanoparticles without doping and after doping with samarium and neodymium. Two synthesis methods, hydrothermal and sol-gel were employed, using titanium tetraisopropoxide (TTIP) as precursor. The TiO_2 nanoparticles obtained were in anatase form using the TTIP precursor. The characterisation techniques, including X-ray diffraction (XRD), scanning electron microscopy (SEM), Fourier-transform infrared spectroscopy (FTIR) and UV-Vis spectroscopy, provided insight into particle size, morphology, crystalline structure and photocatalytic properties. The photocatalytic efficacy was assessed by methylene blue degradation under visible light irradiation. The study reveals distinct doping effects, where Sm and Nd shift TiO_2 absorption edge to the UV region. SEM analysis showed uniform particle distribution with varied morphology depending on synthesis method and the dopants added. XRD data confirmed lattice incorporation of dopants without phase separation. FTIR spectra showed functional groups consistent with rare earth metal-doped TiO_2. Particle sizes, calculated by Scherrer's equation, were generally under 50 nm, with sol-gel and hydrothermal methods affecting crystallinity and agglomeration. This research also underscores the effects of doping for altering the photocatalytic mechanisms and opens avenues for further study into TiO_2-based photocatalysts in environmental and industrial applications.

Keywords: Nanoparticles, Hydrothermal, Sol-gel, Rare earth metals doped TiO_2.

INTRODUCTION

Titanium dioxide (TiO_2) is a stable, non-toxic, low-cost, corrosion resistant and a photocatalytic compound. Owing to this, TiO_2 finds applications in distinct areas like photovoltaic cells, gas sensors, cosmetics, water purification, *etc.* [1,2]. Moreover, it also demonstrates significant optical features that amplify its functional significance [3]. Various synthesis approaches have been established to produce TiO_2 at the nanoscale, with hydrothermal and sol-gel processes being the most often utilized due to their simplicity and good regulation of particle properties [2]. Both methods offer control over the particle size, morphology and crystallinity of TiO_2, which are the essential factors for its applications in areas like solar cells, sensors and photocatalysis. The hydrothermal and sol-gel processes are both very efficient for synthesizing TiO_2 nanoparticles, with the selection of methodology being contingent upon the intended use and the requisite physico-chemical characteristics. Each approach provides distinct benefits regarding particle size regulation, crystallinity and shape; however, they also exhibit particular constraints, rendering method selection a crucial element in customizing TiO_2 nanomaterials [4,5]. Moreover, the hydrothermal results in highly crystalline structure and controlled morphology, while sol-gel is preferred for producing films or coating materials.

TiO_2 nanoparticles exhibit significant absorbance of UV spectrum from solar radiation, in contrast to visible light. To address this deficiency, researchers are endeavoring to create an improved variant of TiO_2 nanoparticles for application as a photocatalyst under visible light [6-9]. There are several ways being reported in the literature for enhancing the photoactivity of TiO_2; one among them is doping with either the metals or the non-metals [10-12]. Some findings have even reported that TiO_2 particles doped with transition metals

show better performance towards the absorbance of the visible light [13-18].

In the present work, the hydrothermal and sol-gel methods were employed to synthesize TiO_2 nanoparticles. Analytical techniques including FTIR, SEM, XRD and UV-Vis spectroscopy, were employed to comprehensively characterize and compare the nanoparticles obtained from each method in terms of their structural, morphological and optical properties. Furthermore, the photocatalytic efficacy of TiO_2 was improved by doping it with rare-earth metals, specifically samarium (Sm) and neodymium (Nd), and the resulting changes in material properties were examined [19].

EXPERIMENTAL

All chemicals employed in this study were of analytical grade and were used as received without any further purification. Glacial acetic acid (99.85% purity) was procured from RFCL Ltd., India, while titanium tetraisopropoxide (TTIP, 97% purity), neodymium oxide and samarium oxide was obtained from Sigma-Aldrich, USA. Sodium hydroxide pellets were sourced from Thermo-Fisher Scientific India Pvt. Ltd., India.

Hydrothermal method: In this case, TiO_2 colloidal solution was prepared by mixing 1 M of TTIP (15.26 mL of TTIP in 50 mL of distilled water) with 4 M of acetic acid (11.466 mL of acetic acid in 50 mL of distilled water) followed by the addition of 10 mL of distilled water and then the whole solution was stirred vigorously for 1 h. After an aging period of 24 h [20], 25 mL of this solution was transferred to stainless steel autoclave and placed in the oven at 180 ºC for 12 h. Autoclave was then allowed to cool down to the room temperature. The solution was taken out from the autoclave for drying at 100 ºC in oven. Dried solid thus obtained was finally crushed to the powder form.

Sol-gel method: The remaining precursor solution prepared for the hydrothermal method was used for the sol-gel method. After an aging period of 24 h, the solution was kept in the oven at 70 ºC to obtain colloidal solution. Afterwards, the solution was dried at 100 ºC and the crystals were crushed to fine powder. Finally, TiO_2 nanoparticles were annealed at 600 ºC for a period of 6 h.

Doping with neodymium and samarium

Neodymium doped TiO_2: In brief, TTIP (6.97 g) dissolved in 20 mL of distilled water was mixed with Nd_2O_3 (0.0833 g dissolved in 20 mL of distilled water) solution at a concentration corresponding to the recommended doping range of 1-10% [21], corresponding to the recommended dopant concentration range of 1-10% followed by the addition of 4 M acetic acid solution and finally the resulting mixture was vigorously stirred for 1 h to ensure the homogeneous dispersion. This solution (25 mL) after going through the aging process of 24 h was transferred to the stainless-steel autoclave and placed in an oven at 180 ºC for 12 h. The solution was dried at 100 ºC to obtain TiO_2 crystals, which was crushed into fine powder with mortar and pestle. The doped nanoparticles thus formed were stored in the airtight container for further use.

Samarium doped TiO_2 nanoparticles: A solution was prepared by mixing TTIP (3.022 mL) in 10 mL distilled water. Separately, 0.035 g of Sm_2O_3 was dissolved in 10 mL distilled water solution and then both the solutions were mixed together. To this mixture, 4 M acetic acid solution was added and then the final liquid solution was stirred vigorously for 1 h and kept aside for aging for 24 h. Finally, 25 mL of this solution was transferred to the stainless-steel autoclave and placed in the oven at 180 ºC for 12 h. The solution was further dried at 100 ºC to obtain TiO_2 nanoparticles and then crushed into fine powder prior to their storage.

Photocatalytic study: The photocatalytic performance of the synthesized nanoparticles was evaluated *via* the degradation of methylene blue (MB) dye in aqueous solution [22]. For this purpose, 0.05 g of TiO_2 nanopowder was dispersed in 50 mL of 20 ppm MB solution and used for the photocatalytic degradation study. The solution was kept under visible light and stirred continuously till the dye was degraded completely. The absorption spectrum of the clear solution was studied *via* UV-Vis spectrophotometer.

RESULTS AND DISCUSSION

XRD studies: The X-ray powder diffraction patterns of the samples were recorded using Cu*K*α (λ = 1.5406 Å) radiation at room temperature in the range of 20 to 80º in the 2θ scale. Fig. 1 depicts the XRD patterns of the samples prepared by TTIP using two different methods *i.e.* hydrothermal and sol-gel methods. The sample obtained after sol-gel method was, further, annealed to determine the effect of heat treatment on the sample. Fig. 1 demonstrates clearly that anatase phase of the TiO_2 nanoparticles was obtained which was confirmed from JCPDS card no. 21-1272 [23]. The strong peaks at 25º (2θ) for all the three samples of nanoparticles confirmed the anatase phase formation of nanoparticles. Another peak at 48º (2θ) and no spurious peaks in the diffraction pattern, further, supports the findings of the anatase structure of TiO_2 particles [23-26]. Also, the peaks intensity revealed crystallinity of the nanoparticles and broadened peaks highlighted small sized crystals of the nanoparticles [23]. Further, anatase phase nanopowders had tetragonal structure, which generally exhibits higher catalytic activity [27,28]. It was concluded that the hydrothermal method resulted in the formation of larger particles than the sol-gel method. However, heat treatment of nanoparticles obtained from sol-gel method resulted in the further growth of their size although the phase remained the same. In addition, the peak intensity of anatase phase was increased with the calcination temperature.

To improve the photocatalytic properties, hydrothermally synthesised TiO_2 nanoparticles were doped with the rare earth metals (Sm and Nd). Fig. 2 exhibits XRD patterns of rare earth metals doped TiO_2 nanoparticles that clearly depicts that no separate peaks were obtained after doping, which could be due to the fact that the doped metals were incorporated well in the lattice sites of TiO_2. Further, peak intensity at 101 plane depicted slight decrease for the rare earth doped samples in comparison to the undoped sample. This decrease was attributed to the presence of RE-O-Ti (RE = Sm or Nd) in the doped samples, which could have inhibited the growth of the crystal grains [29-31].

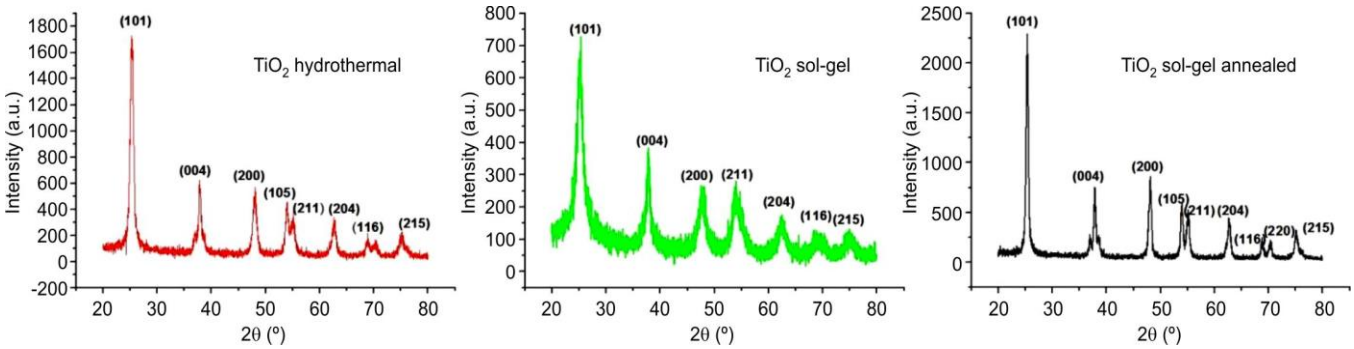

Fig. 1. XRD patterns of hydrothermal (a) sol-gel (b) and thermally treated TiO_2 nanoparticles synthesised using TTIP

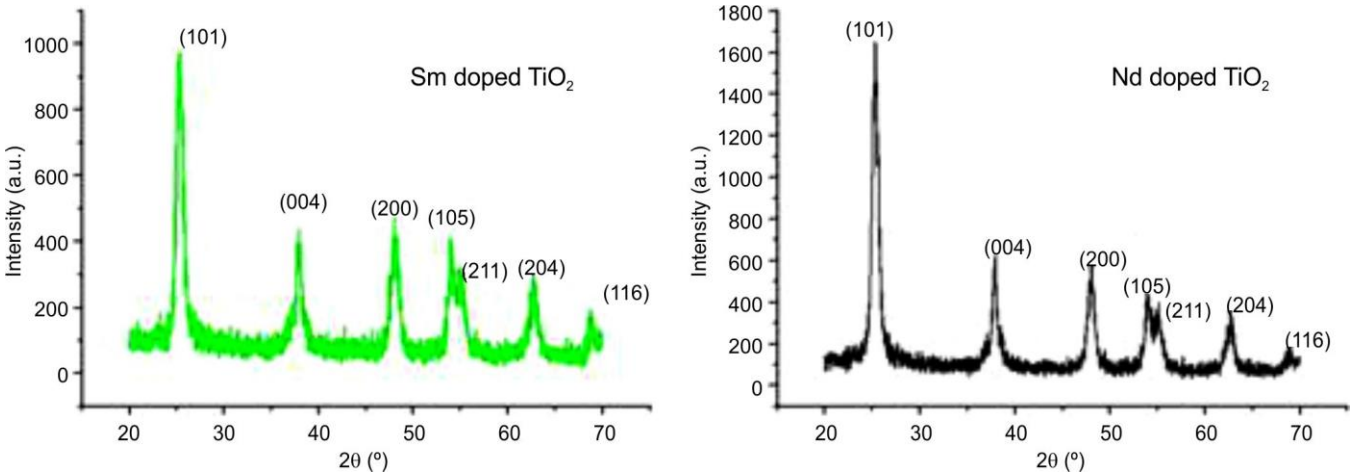

Fig. 2. XRD patterns of Sm and Nd-doped TiO_2 nanoparticles

The size of the particles was calculated using Debye-Scherrer's equation presented below [23]:

$$D = \frac{0.9\lambda}{\beta \cos\theta}$$

where D = particle size (nm); β = FWHM (full width at half maximum); λ = wavelength of X-ray (0.154 nm); and θ = Bragg's diffraction angle. Using Debye-Scherrer equation, particles size of all the synthesised undoped and doped TiO_2 nanoparticles was evaluated.

It was observed from Table-1 that the maximum size of the nanoparticles was quite less than 20 nm [10]. Further, the size of the nanoparticles formed by hydrothermal method is more than the sol-gel method. Upon heating the nanoparticles at 600 ºC prepared by the sol-gel method produced bigger particles of size 15.28 nm in contrast to 4.48 nm of nanoparticles without heat treatment which might be due to the sintering effect [13,25]. It is already reported [13,14,32] that doping with rare-earth metals such as Sm and Nd is expected to interfere with the crystal growth, leading to a slight reduction in nanoparticle size, which is found consistent with the present results.

SEM studies: The morphological structure of different nanoparticles of TiO_2 prepared by various methods has been exhibited in Figs. 3 and 4. The overall morphology of the samples showed uniform thickness and good homogeneity with smooth interface having perfect regular shape. The round shaped particles structure further confirms the anatase form

TABLE-1
PARTICLE SIZE OF TiO_2 NANOPARTICLES CALCULATED USING SCHERRER's EQUATION FOR VARIOUS SYNTHETIC METHODS AND ITS DOPED SAMPLES

Sample	2θ	FWHM	Crystal size (nm)
TiO_2 (TTIP) hydrothermal	25.2920	0.78130	10.4
TiO_2 sol-gel	25.1720	1.82050	4.5
TiO_2 sol-gel annealed	25.3594	0.53318	15.3
Sm-doped TiO_2	25.3700	0.88100	9.3
Nd-doped TiO_2	25.3200	0.84200	9.7

[26]. SEM analysis revealed that the particles were uniformly distributed with partial agglomeration, while no evidence of contamination was observed in the samples [18].

FTIR spectral studies: Fig. 5 shows the FTIR spectrum of undoped TiO_2 nanoparticles, in which a broad absorption band observed in the range of 3440-3400 cm^{-1} corresponds to –OH stretching vibrations present in all samples [32-34]. The band at 2926 cm^{-1} is attributed to Ti–O stretching vibrations, while the strong absorption band around 700 cm^{-1} is characteristic of Ti–O stretching and Ti–O–Ti bridging modes [35]. The peaks present in all the four samples near 1630 cm^{-1} could be due to the bending vibrations of adsorbed H_2O molecules [32,36,37]. Furthermore, the peaks at 1412 cm^{-1}, 1422 cm^{-1}, 1384 cm^{-1} present in TiO_2 hydrothermal, TiO_2 sol-gel and TiO_2 sol-gel annealed samples, respectively, were due to Ti-O-Ti. The characteristic vibrations present between 600

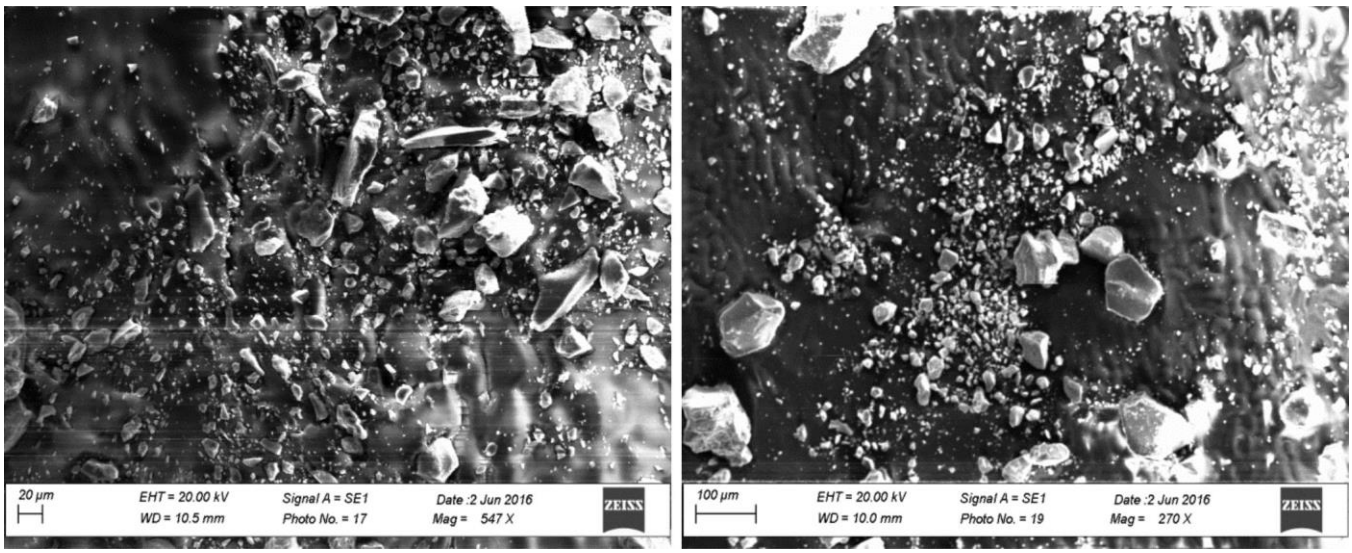

Fig. 3. SEM images of TiO_2 nanoparticles synthesised hydrothermally with TTIP precursor

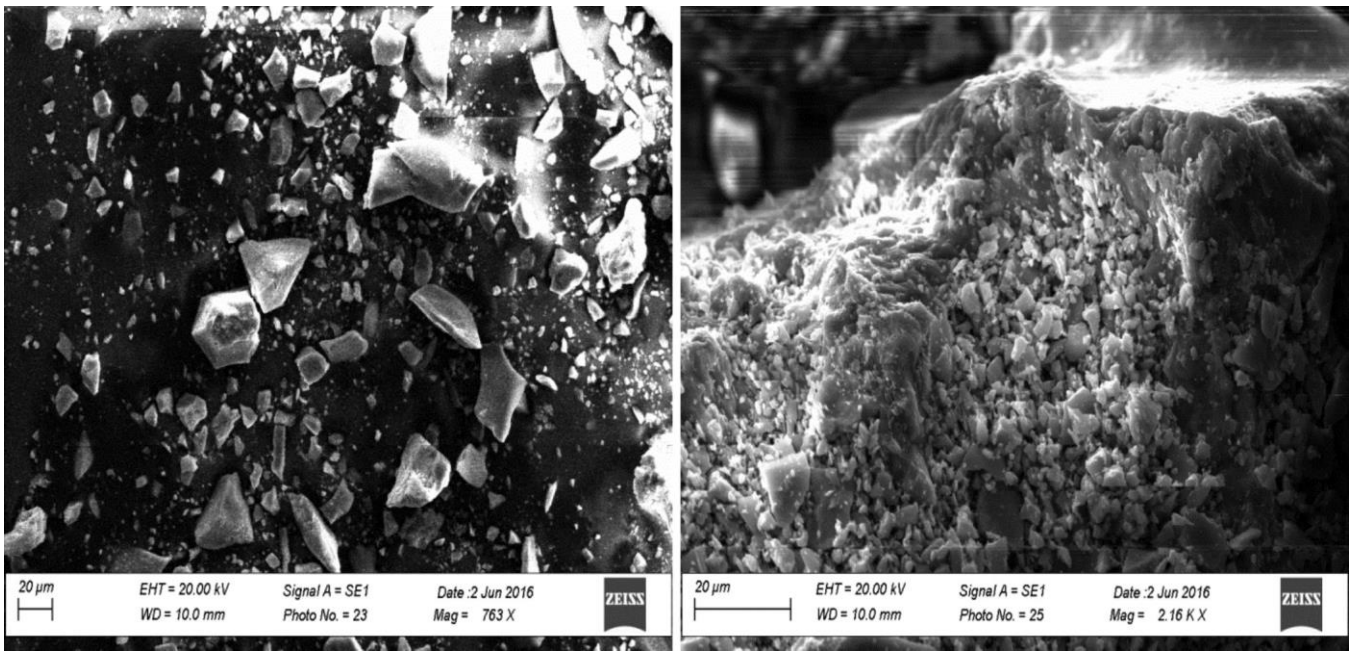

Fig. 4. SEM images of TiO_2 nanoparticles synthesised by sol-gel method after annealing

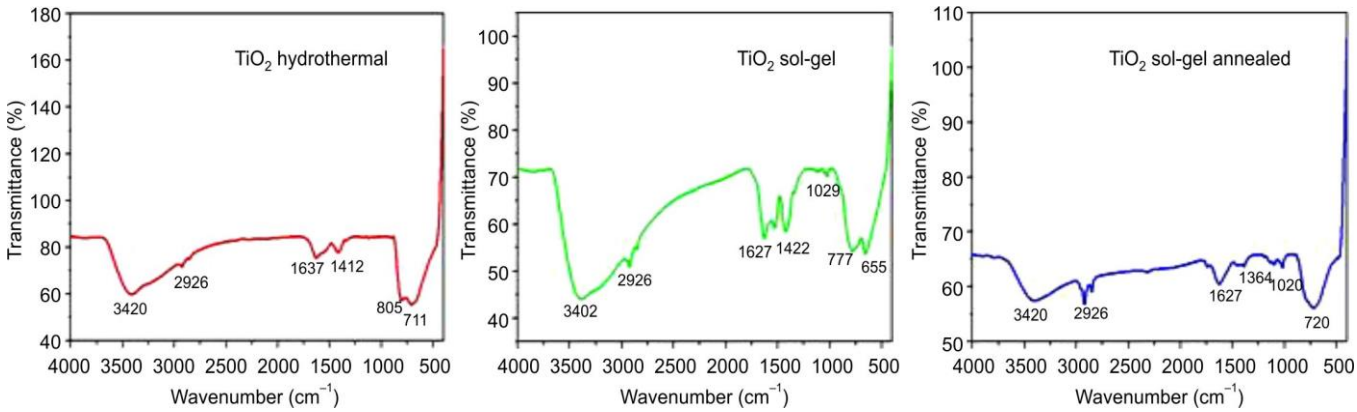

Fig. 5. FTIR spectra of hydrothermal (a), sol-gel (b) synthesised and thermal (c) treated undoped TiO_2 nanoparticles

and 800 cm^{-1} are due to the inorganic Ti-O stretching [35]. The bands of Ti-O confirmed the formation of TiO_2 nanoparticles. After the heat treatment of the sample, the water adsorption on sample surface decreased as depicted in the FTIR spectrum of the annealed sample.

Fig. 6 presents the FTIR spectra of the samples *i.e.* rare earth metals (Nd and Sm) doped TiO_2. In all the samples, the vibration due to –OH stretching was present near 3400 cm^{-1} [33,34]. The bending due to adsorption of water was observed at 1627 cm^{-1}, 1637 cm^{-1} and 1627 cm^{-1}, respectively, in the FTIR spectrum of the metal doped nanoparticles [36,37]. Small bands present at 1431 cm^{-1} and 1422 cm^{-1} indicated the Ti-O vibrations, stated elsewhere [35].

UV-Vis spectral studies: The UV-Vis spectrum of nanoparticles prepared by hydrothermal and sol-gel methods are presented in Fig. 7. Anatase phase depicted absorption band near 350 nm, which originated primarily from the absorption and scattering of UV radiation by TiO_2 nanoparticles [38,39]. There was an absorption band near 350 nm for the nanoparticles prepared hydrothermally indicative of anatase form of nanoparticles [25]. The absorption was comparatively low among the nanoparticles produced in the sol-gel method though it increased considerably after the heat treatment. After the heat treatment at 600 ºC, the absorption band was shifted towards the visible region and was present near 400 nm. This suggests that the hydroxyl groups were removed after the heat treatment resulting in better performance in the UV and visible regions.

Fig. 8 indicates that upon doping with Nd and Sm, the absorption edge shifted toward the UV region, with the doped nanoparticles exhibiting absorption edges near 320 nm and 300 nm, respectively. This shift suggests that doping with both rare-earth metals exerted a negative effect by moving the absorption edge further into the UV region.

Degradation studies: The photocatalytic property of the undoped and rare earth doped TiO_2 nanoparticles was predicted through its ability towards degradation of methylene blue (MB) dye. The experiments were conducted with all the samples of nanoparticles which showed different time scale for the degradation of MB dye from its aqueous solution. Nd doped TiO_2 showed similar performance towards the degradation of the dye molecules as presented in Fig. 9. The dye was completely degraded after 12 min of addition of TiO_2 nanoparticles to the MB dye solution. The dye samples were taken at different time intervals and the initial dye solution was taken as reference sample. As a result, a progressive decre-

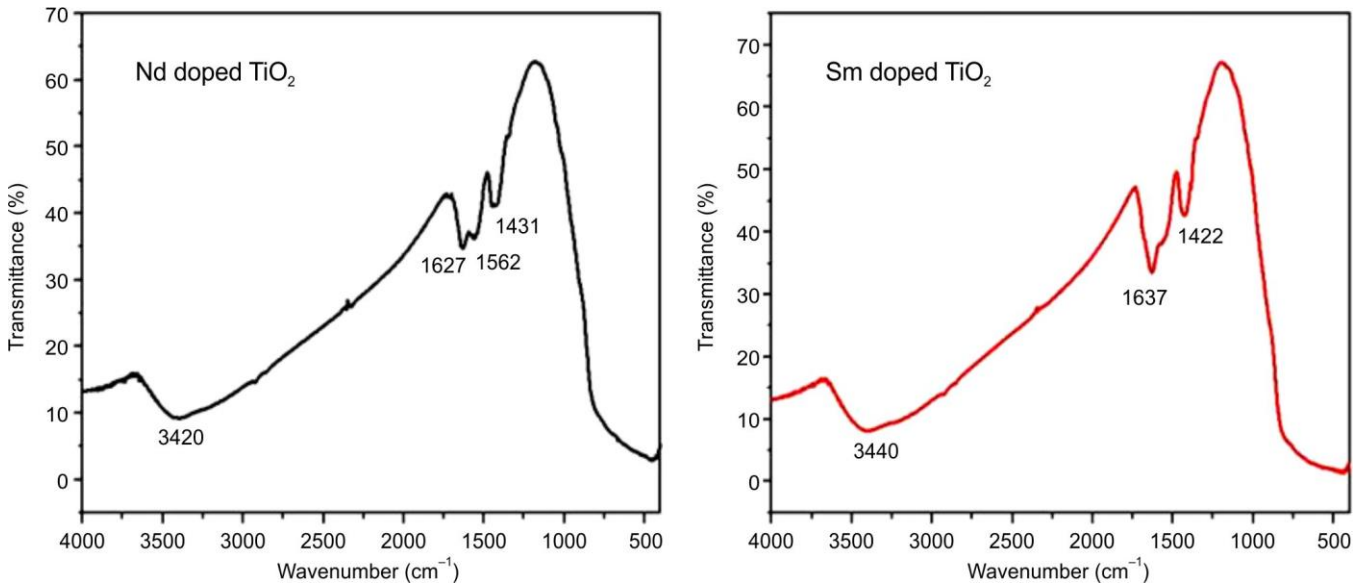

Fig. 6. FTIR spectra of Sm and Nd-doped TiO_2 nanoparticles

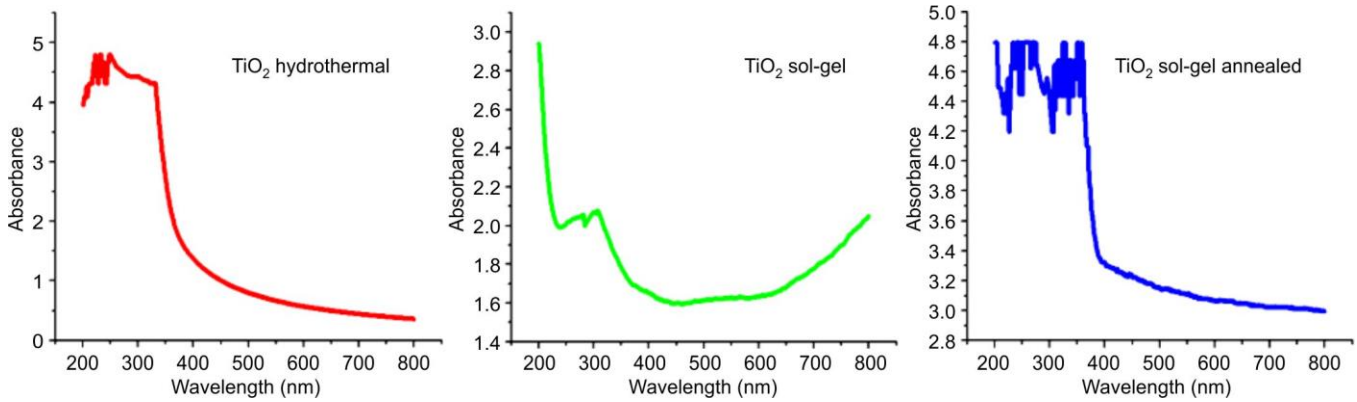

Fig. 7. UV-Vis spectra of hydrothermal (a) and sol-gel (b) synthesised TiO_2 nanoparticles with thermal treatment (c)

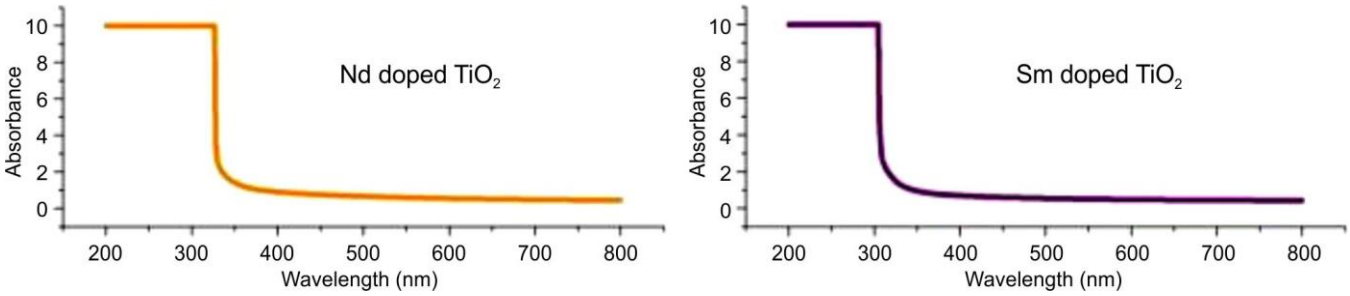

Fig. 8. UV-Vis spectra of Nd and Sm-doped TiO_2 nanoparticles, highlighting the shifts in absorption edge towards the UV region

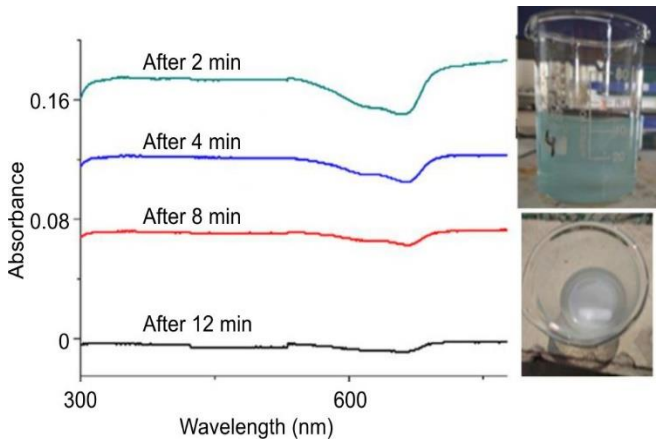

Fig. 9. UV-Vis spectra of methylene blue degradation using Nd-doped TiO_2 nanoparticles at different interval of times

ase in absorbance at around 668 nm, corresponding to MB dye degradation, was observed. This decline became more pronounced with increasing irradiation time, ultimately indicating near-complete degradation of the dye. The final solution did not appear clear or transparent, likely due to the formation of a colloidal suspension of TiO_2 nanoparticles in water.

Similar behaviour was observed for the Sm-doped sample, as shown in Fig. 10, where TiO_2 nanoparticles doped with Sm facilitated rapid degradation of methylene blue dye within 10 min. A distinct decrease in absorbance near 670 nm was recorded, confirming the degradation of the dye molecules.

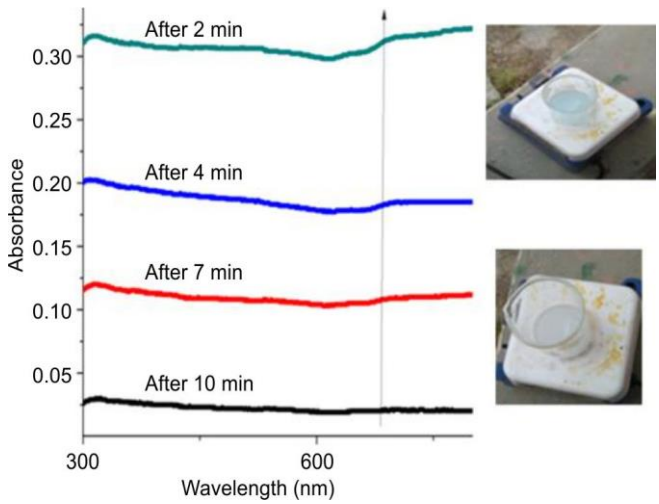

Fig. 10. UV-Vis spectra of methylene blue degradation using Sm-doped TiO_2 nanoparticles at different interval of times

The synthesised undoped TiO_2 nanoparticles demonstrated the exceptional photocatalytic efficiency, achieving complete degradation of methylene blue (MB) dye within approximately 12 min under visible light irradiation. This rapid degradation rate is notably superior to those reported in recent studies. For instance, a study on brookite-rutile TiO_2 composites reported complete MB degradation after 3 h under UV light and 36 h under visible light [40]. Another investigation involving Ag-doped TiO_2 achieved 80% MB degradation after 12 h of visible light exposure [41]. Contrary to expectations, doping TiO_2 with samarium (Sm) and europium (Eu) resulted in reduced photocatalytic performance [42]. This decline can be attributed to several factors like (i) formation of recombination centers as the incorporation of Sm^{3+} and Nd^{3+} ions may introduce defect sites within the TiO_2 lattice, acting as recombination centers for photo-generated electron-hole pairs, thereby diminishing the availability of charge carriers essential for photocatalytic reactions; (ii) alteration of electronic structure when rare-earth doping created the localised energy states within the TiO_2 band gap. While this modification has the potential to enhance visible light absorption, which may also facilitate non-radiative recombination processes, adversely impacting the photocatalytic efficiency and finally (iii) impact of the crystallinity and surface area, where the doping process can affect the crystallinity and surface morphology of TiO_2 nanoparticles.

Conclusion

This study demonstrates that undoped TiO_2 nanoparticles, synthesised *via* hydrothermal and sol-gel methods, exhibit rapid and efficient photocatalytic degradation of methylene blue dye under visible light irradiation, achieving complete degradation within approximately 12 min. When commercially available TiO_2 powder is used as the precursor, rutile-phase TiO_2 nanoparticles are typically obtained, as reported in previous studies, whereas the use of titanium tetraisopropoxide (TTIP) as the precursor preferentially leads to the formation of anatase-phase TiO_2 nanoparticles. Furthermore, nano-TiO_2 was doped with samarium and neodymium to prepare three different compositions with the aim to test their photocatalytic ability in the visible region. However, doping with Nd and Sm with did not enhance as in some cases diminished the photocatalytic performance. The photocatalytic activities of Nd and Sm doped TiO_2 nanoparticles show very small changes in MB dye degradation rates under solar irradiation. This suggests that the introduction of these rare-earth dopants may create recombination centers or alter the electronic structure in ways detrimental to the photocatalysis.

CONFLICT OF INTEREST

The authors declare that there is no conflict of interests regarding the publication of this article.

DECLARATION OF AI-ASSISTED TECHNOLOGIES

During the preparation of this manuscript, the authors used an AI-assisted tool(s) to improve the language. The authors reviewed and edited the content and take full responsibility for the published work.

REFERENCES

1. R. Nankya and K.N. Kim, *J. Nanosci. Nanotechnol.*, **16**, 11631 (2016); https://doi.org/10.1166/jnn.2016.13564
2. F. Giuffrida, L. Calcagno, A.A. Leonardi, M. Cantarella, M. Zimbone and G. Impellizzeri, *Thin Solid Films*, **771**, 139783 (2023); https://doi.org/10.1016/j.tsf.2023.139783
3. H.N.C. Dharma, J. Jaafar, N. Widiastuti, H. Matsuyama, S. Rajabsadeh, M.H.D. Othman, M.A. Rahman, N.N.M. Jafri, N.S. Suhaimin, A.M. Nasir and N.H. Alias, *Membranes*, **12**, 345 (2022); https://doi.org/10.3390/membranes12030345
4. C.Z. Costa, E.F. Sousa-Aguiar, M.A.P.G. Couto and J.F.S. de C. Filho, *Catalysts*, **10**, 843 (2020); https://doi.org/10.3390/catal10080843
5. L. Cano-Casanova, A. Amorós-Pérez, M.Á. Lillo-Ródenas and M.C. Román-Martínez, *Materials*, **11**, 2227 (2018); https://doi.org/10.3390/ma11112227
6. S.K. Arla, S.K. Godlaveeti, S.S. Sana, A. Jwuiyad, N.S.S. Konidena and V.K.N. Boya, *J. Solid State Electrochem.*, **28**, 2035 (2024); https://doi.org/10.1007/s10008-023-05720-6
7. N. khan, A. Sapi, I. Arora, S. Sagadevan, A. Chandra and S. Garg, *React. Kinet. Mech. Catal.*, **137**, 629 (2024); https://doi.org/10.1007/s11144-024-02601-5
8. C. Song, L. Xiao, Y. Chen, F. Yang, H. Meng, W. Zhang, Y. Zhang and Y. Wu, *Catalysts*, **14**, 366 (2024); https://doi.org/10.3390/catal14060366
9. S. Ali, P.M. Ismail, M. Khan, A. Dang, S. Ali, A. Zada, F. Raziq, I. Khan, M.S. Khan, M. Ateeq, W. Khan, S.H. Bakhtiar, H. Ali, X. Wu, M.I.A. Shah, A. Vinu, J. Yi, P. Xia and L. Qiao, *Nanoscale*, **16**, 4352 (2024); https://doi.org/10.1039/D3NR04534J
10. D. De Angelis, F. Presel, N. Jabeen, L. Bignardi, D. Lizzit, P. Lacovig, S. Lizzit, T. Montini, P. Fornasiero, D. Alfè and A. Baraldi, *Carbon*, **157**, 350 (2020); https://doi.org/10.1016/j.carbon.2019.10.053
11. P.S. Basavarajappa, S.B. Patil, N. Ganganagappa, K.R. Reddy, A.V. Raghu and C V. Reddy, *Int. J. Hydrogen Energy*, **45**, 7764 (2020); https://doi.org/10.1016/j.ijhydene.2019.07.241
12. H. Almohamadi, S.A. Awad, A.K. Sharma, N. Fayzullaev, A. Távara-Aponte, L. Chiguala-Contreras, A. Amari, C. Rodriguez-Benites, M.A. Tahoon and H. Esmaeili, *Catalysts*, **14**, 420 (2024); https://doi.org/10.3390/catal14070420
13. P. Karuppasamy, N. R. N. Nisha, A. Pugazhendhi, S. Kandasamy, and S. Pitchaimuthu, *J. Environ. Chem. Eng.*, **9**, 105254 (2021); https://doi.org/10.1016/j.jece.2021.105254
14. A. Aljaafari, *Curr. Nanosci.*, **18**, 499 (2022); https://doi.org/10.2174/1573413717666210706115018
15. K.A. Rahman, T. Bak, A. Atanacio, M. Ionescu and J. Nowotny, *Ionics*, **24**, 327 (2018); https://doi.org/10.1007/s11581-017-2370-9
16. M. Zimbone, G. Cacciato, L. Spitaleri, R.G. Egdell, M.G. Grimaldi and A. Gulino, *ACS Omega*, **3**, 11270 (2018); https://doi.org/10.1021/acsomega.8b01452
17. G. Impellizzeri, V. Scuderi, L. Romano, P.M. Sberna, E. Arcadipane, R. Sanz, M. Scuderi, G. Nicotra, M. Bayle, R. Carles, F. Simone and V. Privitera, *J. Appl. Phys.*, **116**, 173507 (2014); https://doi.org/10.1063/1.4901208
18. H. Mansour, M. Madani, Fatemah M. Barakat, K. Omri, B.B. Alyahya, F. Alharbi and S. Gouadria, *Transition Met. Chem.*, **50**, 61 (2025); https://doi.org/10.1007/s11243-024-00605-7
19. S.S. Mohtar, F. Aziz, A.F. Ismail, N.S. Sambudi, H. Abdullah, A.N. Rosli and B. Ohtani, *Catalysts*, **11**, 1160 (2021); https://doi.org/10.3390/catal11101160
20. U.M. Aliyu, S. Rathilal, S.I. Mustapha, R. Musamali and E.K. Tetteh, *Catal. Commun.*, **182**, 106750 (2023); https://doi.org/10.1016/j.catcom.2023.106750
21. N. Munna, R. Abdur, R. Islam, M.S. Bashar, S.F.U. Farhad, M. Kamruzzaman, S. Aziz, M.A.A. Shaikh, M. Hossain and M.S. Jamal, *Nanoscale Adv.*, **5**, 4996 (2023); https://doi.org/10.1039/D3NA00409K
22. A.K.M.A. Habib, K.M.R. Rifat, M.E. Kabir, J.N. Khan, S.M.N. Rokon and M.A. Rabbi, *Results Mater.*, **22**, 100581 (2024); https://doi.org/10.1016/j.rinma.2024.100581
23. W. Li, R. Liang, A. Hu, Z. Huang and Y.N. Zhou, *RSC Adv.*, **4**, 36959 (2014); https://doi.org/10.1039/C4RA04768K
24. Ž. Antić, R.M. Krsmanović, M.G. Nikolić, M. Marinović-Cincović, M. Mitrić, S. Polizzi and M.D. Dramićanin, *Mater. Chem. Phys.*, **135**, 1064 (2012); https://doi.org/10.1016/j.matchemphys.2012.06.016
25. M.M. Ba-Abbad, A.A.H. Kadhum, A.B. Mohamad, M.S. Takriff and K. Sopian, *Int. J. Electrochem. Sci.*, **7**, 4871 (2012); https://doi.org/10.1016/S1452-3981(23)19588-5
26. K. Thamaphat, P. Limsuwan and B. Ngotawornchai, *Witthayasan Kasetsat Witthayasat*, **42**, 357 (2008).
27. F. Sahara, M. Sultana, K. Amin, M. Mamun, P. Dhar and S. Dutta, *ChemistryOpen*, **14**, e202400277 (2024); https://doi.org/10.1002/open.202400277
28. T. Luttrell, S. Halpegamage, J. Tao, A. Kramer, E. Sutter and M. Batzill, *Sci. Rep.*, **4**, 4043 (2014); https://doi.org/10.1038/srep04043
29. C.-C. Tsai and H. Teng, *Chem. Mater.*, **16**, 4352 (2004); https://doi.org/10.1021/cm049643u
30. R. Ma, Y. Bando and T. Sasaki, *Chem. Phys. Lett.*, **380**, 577 (2003); https://doi.org/10.1016/j.cplett.2003.09.069
31. X. Sun and Y. Li, *Chemistry*, **9**, 2229 (2003); https://doi.org/10.1002/chem.200204394
32. A. Wafi, L. Roza, G.E. Timuda, D. Aji, D.S. Khaerudini, N. Darsono, N. Yudasari, E. Szabó-Bárdos, O. Horváth and M.M. Khan, *Transition Met. Chem.*, **49**, 305 (2024); https://doi.org/10.1007/s11243-024-00584-9
33. K.L. Yeung, S.T. Yau, A.J. Maira, J.M. Coronado, J. Soria and P.L. Yue, *J. Catal.*, **219**, 107 (2003); https://doi.org/10.1016/S0021-9517(03)00187-8
34. X. Chen, X. Wang, Y. Hou, J. Huang, L. Wu and X. Fu, *J. Catal.*, **255**, 59 (2008); https://doi.org/10.1016/j.jcat.2008.01.025
35. D. Huang, S. Liao, S. Quan, L. Liu, Z. He, J. Wan and W. Zhou, *J. Mater. Res.*, **22**, 2389 (2007); https://doi.org/10.1557/jmr.2007.0319
36. J. Geng, D. Yang, J. Zhu, D. Chen and Z. Jiang, *Mater. Res. Bull.*, **44**, 146 (2009); https://doi.org/10.1016/j.materresbull.2008.03.010
37. M. Primet, P. Pichat and M.V. Mathieu, *J. Phys. Chem.*, **75**, 1216 (1971); https://doi.org/10.1021/j100679a007
38. M. Niu, R. Cui, H. Wu, D. Cheng and D. Cao, *J. Phys. Chem. C*, **119**, 13425 (2015); https://doi.org/10.1021/acs.jpcc.5b02652
39. C.-S. Chou, Y.-H. Huang, P. Wu and Y.-T. Kuo, *Appl. Energy*, **118**, 12 (2014); https://doi.org/10.1016/j.apenergy.2013.12.012
40. M.G. Kim, J.E. Lee, K.S. Kim, J.M. Kang, J.H. Lee, K.H. Kim, M. Cho and S.G. Lee, *New J. Chem.*, **45**, 3485 (2021); https://doi.org/10.1039/D0NJ05162D
41. M. Khan, S.R. Gul, J. Li and W. Cao, *J. Miner. Met. Mater. Soc.*, **67**, 2104 (2015); https://doi.org/10.1007/s11837-015-1486-5
42. R.A. Zargar, M. Imran, M. Arora, V. Nagal, M.A. Manthrammel, T. Mearaj, M. Shkir and A.K. Hafiz, *J. Mater. Sci. Mater. Electron.*, **33**, 26931 (2022); https://doi.org/10.1007/s10854-022-09357-5